Available online at www.sciencedirect.com
ScienceDirect
Trans. Nonferrous Met. Soc. China 30(2020) 2879−2890
Transactions of Nonferrous Metals Society of China
www.tnmsc.cn

Effect of Sr modification on microstructure and thermal conductivity of hypoeutectic Al−Si alloys

Jun-qi GAN, Yu-jian HUANG , Cheng WEN, Jun DU

School of Materials Science and Engineering, South China University of Technology, Guangzhou 510640, China

Received 23 January 2020; accepted 4 September 2020

Abstract: Trace amount of Sr (0.05 wt.%) was added into the hypoeutectic Al−Si (3−12 wt.% Si) alloys to modify their microstructure and improve thermal conductivity. The results showed that the thermal conductivity of hypoeutectic Al−Si alloys was improved by Sr modification, and the increment and increasing rate of the thermal conductivity gradually increased with Si content increasing. The improvement of thermal conductivity was primarily related to the morphology variation of eutectic Si phases. In Sr-modified Al−Si alloys, the morphology of eutectic Si phases was a mixed morphology of fiber structure and fine flaky structure, and the proportion of the fine flaky eutectic Si phases gradually decreased with Si content increasing. Under the Si content reaching 9 wt.%, the proportion of fine flaky eutectic Si phases was nearly negligible in Sr-modified alloys. Correspondingly, the increment and increasing rate of thermal conductivity of Sr-modified alloys reached the maximum and tended to be stable.

Key words: hypoeutectic Al−Si alloy; Sr modification; eutectic Si morphology; thermal conductivity; Al/Si interface

1 Introduction

Nowadays, some novel industries of 5G communication and new energy vehicles are being rapidly developed. The heat dissipation performance of materials that are applied in the sealed cavity housing of radio remote unit (RRU) of 5G communication base station and the battery pack cooling module of the new energy vehicle has received wide attention in the above mentioned emerging industries. The die-casting process of Al alloys is the most common technology to manufacture these components. Therefore, the research on die-casting Al alloys with high thermal conductivity has an important engineering significance and application value [1,2].

Al−Si alloys are the most commonly used die-casting Al alloys. However, the electrical conductivity of Al alloys would decrease with the addition of Si [3]. The reduction percentage of electrical conductivity of Al for Si in the state of solid solution was 11.6 times that of Si in the state of non-solid solution [4]. The equilibrium solid solubility of Si in Al matrix is only 0.05 wt.% at room temperature. Hence, the amount of Si in the state of non-solid solution is more than that of Si in the state of solid solution when the Si content is far more than 0.05 wt.% in Al alloys. As a result, the effect of Si in the state of non-solid solution on the electrical conductivity is also significantly important in most commercial Al−Si alloys. According to Weizmann−Frantz law [5,6], the electrical conductivity of alloys is normally proportional to the thermal conductivity. Therefore, the effect of Si on the electrical conductivity of Al alloys will be as same as that on the thermal conductivity of Al alloys.

In hypoeutectic Al−Si alloys, most of non-solid solution Si exists in the form of eutectic Si

Foundation item: Project (2013B090500091) supported by Industry-University-Research Combined Project of Guangdong Province, China; Project (20180358) supported by the Shenzhen Jiansheng Technology Inc. Cooperation Project, China
Corresponding author: Jun DU; Tel: +86-20-87113597; Fax: +86-20-87113597; E-mail: tandujun@sina.com
DOI: 10.1016/S1003-6326(20)65428-0

phases. In order to improve the strengthening effect of eutectic Si phases, researchers have studied many modified processes [7−9]. At present, the Sr modification process is widely used to treat the Al−Si alloys because Sr can efficiently transform the eutectic Si phases from coarse flaky structure to fine fiber structure, and improve the mechanical properties of Al−Si alloys [10−12]. In addition, some researchers have also found that Sr modification process can also improve the thermal conductivity of hypoeutectic Al−Si alloys, and believed that the transformation of eutectic Si morphology is the main reason for the improvement of thermal conductivity [13,14]. However, the mechanism of eutectic Si morphology affecting thermal conductivity has not been studied in depth.

Some researchers adopted the Maxwell model [15] to delve into the thermal conductivity of unmodified Al−Si alloys and compared the theoretical values. Besides, it was reported that the model can help qualitatively determine the varying trend of the thermal conductivity [5,6,16]. However, rare studies have been conducted to analyze the thermal conductivity of Sr-modified Al−Si alloys with Maxwell model. Some researchers reported that the morphology of the eutectic Si phases showed a direct association with the thermal conductivity of Sr-modified Al−Si alloys [17,18]. However, in the Maxwell model the effect of the second phase morphology on the thermal conductivity was not considered. For this reason, other methods should be adopted to analyze the variation law of the thermal conductivity of Al−Si alloys modified by Sr.

In this work, the hypoeutectic Al−Si alloys were selected as the model materials. The effect of Sr modification process on the morphology of eutectic Si phases in hypoeutectic Al−Si alloys with different Si contents was analyzed in depth. By establishing the free electrons scattering model at the Al/Si interface, the mechanism of thermal conductivity change was deeply studied.

2 Experimental

The commercially pure Al (99.8 wt.% Al, 0.095 wt.% Fe, 0.035 wt.% Si, 0.02 wt.% Zn, etc.) and Al−20Si master alloy were used as raw materials to prepare Al−Si binary alloys with different Si contents (0, 3, 5, 7, 9, and 12 wt.%). The raw materials were placed in graphite clay crucible and then melted in an electric resistance furnace (SG2−5−10). The melting temperature was set to be 750 °C. After melting, the melt was modified by Al−10Sr master alloy, and the addition amount of Sr was 0.05 wt.%. Subsequently, the melt was poured into a steel mold preheated at 200 °C to obtain a casting with a thickness of 4 mm. The castings air-cooled after pouring and all alloys were subjected to the identical solidification and cooling conditions.

The as-cast samples were processed into cylinders (d12.7 mm × 3 mm) and then employed to determine the thermal diffusivity (α) with the laser flash method (NDTZSCH DSC 204F1) at room temperature [19]. The sample density was determined with Archimedes method (GF300-D). Besides, the specific capacity was measured with a differential scanning calorimeter (Netzsch DSC). At last, the thermal conductivity (λ) of each alloy was calculated by the formula: $\lambda=\alpha\rho c_p$ [20].

In order to characterize the three-dimensional morphology of eutectic Si phases, the samples were deep-etched with 10% hydrochloric acid alcohol for about 20 min, and then the surface of the samples was washed with absolute alcohol. Lastly, the eutectic Si phases were characterized by SEM−SEI (ZEISS Merlin).

3 Results

3.1 Thermal conductivity

The density (ρ), thermal diffusivity (α), specific heat capacity (c_p) and thermal conductivity (λ) of each alloy were listed in Table 1. Since commercially pure Al contains impurities, the thermal conductivity of commercially pure Al (230.6 W/(m·K)) is lower than that of high purity Al (237 W/(m·K)). When Al−Si alloys were modified by Sr, the thermal conductivity (λ) increased. The increment ($\Delta\lambda$, $\Delta\lambda=\lambda_{md}-\lambda_{unmd}$, λ_{md} is the thermal conductivity of Sr-modified alloy, λ_{unmd} is the thermal conductivity of unmodified alloy) and increasing rate ($\Delta\lambda/\lambda_{unmd}$) of thermal conductivity were calculated, as listed in Table 1.

Figure 1 showed the effect of Si content on the thermal conductivity of unmodified and Sr-modified Al−Si alloys. Figure 1(a) indicated that

Table 1 Thermal conductivities and related properties of Al and its alloys

Alloy	ρ/ ($g\cdot cm^{-3}$)	α/ ($mm^2\cdot s^{-1}$)	c_p/ ($J\cdot g^{-1}\cdot K^{-1}$)	λ/ ($W\cdot m^{-1}\cdot K^{-1}$)	$\Delta\lambda$/ ($W\cdot m^{-1}\cdot K^{-1}$)	$(\Delta\lambda/\lambda_{unmd})$/ %
Pure Al	2.709	95.967	0.887	230.6		
Al−0.05Sr	2.701	94.921	0.889	227.9	−2.7	−1.2
Al−3Si	2.662	83.083	0.781	172.8		
Al−3Si−0.05Sr	2.628	82.592	0.848	184.1	11.2	6.5
Al−5Si	2.629	79.797	0.765	160.5		
Al−5Si−0.05Sr	2.659	78.011	0.844	175.1	14.6	9.1
Al−7Si	2.674	69.392	0.747	138.6		
Al−7Si−0.05Sr	2.659	75.720	0.842	169.6	30.4	21.9
Al−9Si	2.678	68.361	0.720	131.8		
Al−9Si−0.05Sr	2.687	72.934	0.842	165.0	33.2	25.2
Al−12Si	2.624	69.045	0.709	128.4		
Al−12Si−0.05Sr	2.691	72.620	0.829	161.2	32.8	25.5

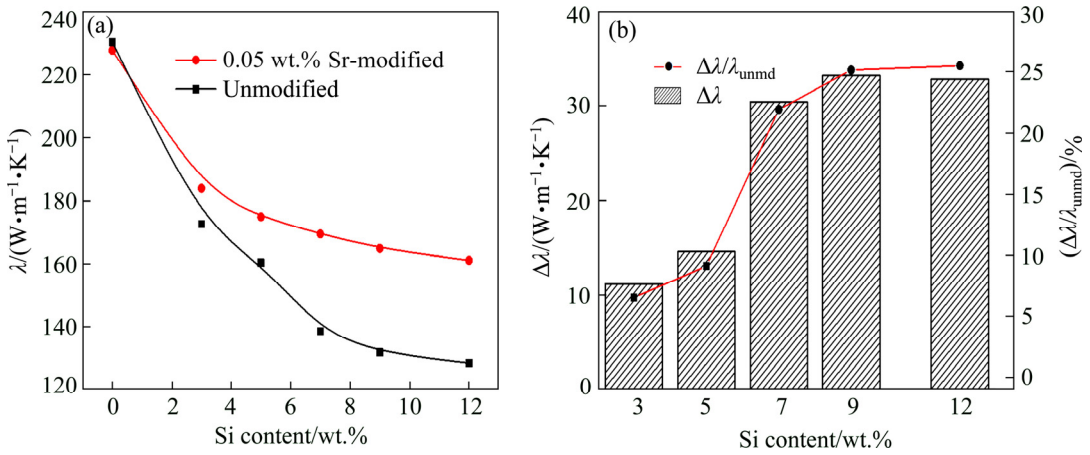

Fig. 1 Effect of Si content on thermal conductivity of Sr-modified and unmodified Al−Si alloys (a), and improvement of thermal conductivity induced by Sr modification (b)

the thermal conductivity of unmodified Al−Si alloys gradually decreased by the addition of Si. The decline rate of thermal conductivity of Sr-modified Al−Si alloys was lower than that of unmodified Al−Si alloys. With the Si content increasing, the difference in thermal conductivity between unmodified and Sr-modified Al−Si alloys gradually increased.

The columnar height in Fig. 1(b) indicated the increment of the thermal conductivity of Sr-modified Al−Si alloys, and the curve showed the trend of the increasing rate of thermal conductivity ($\Delta\lambda/\lambda_{unmd}$) of Sr-modified Al−Si alloys. Figure 1(b) showed that the thermal conductivity of hypoeutectic Al−Si alloys was improved by Sr modification process. In general, the increment and the increasing rate of thermal conductivity were improved with the Si content increasing, and were stabilized at Si content of 9 wt.%. When the Si content was 3 wt.%, the increment and increasing rate of the thermal conductivity were the lowest, only 11.2 W/(m·K) and 6.5%, respectively. When the Si content was 9 wt.%, the increment and increasing rate of the thermal conductivity were 33.5 W/(m·K) and 25.2%, respectively, and tended to be stable as Si content further increased.

3.2 Microstructure

The microstructure of hypoeutectic Al−Si alloys is composed of primary α(Al) and (α(Al)+Si) eutectic structure. Figure 2 showed the OM images of Sr-modified Al−Si alloys. From Fig. 2 it can be

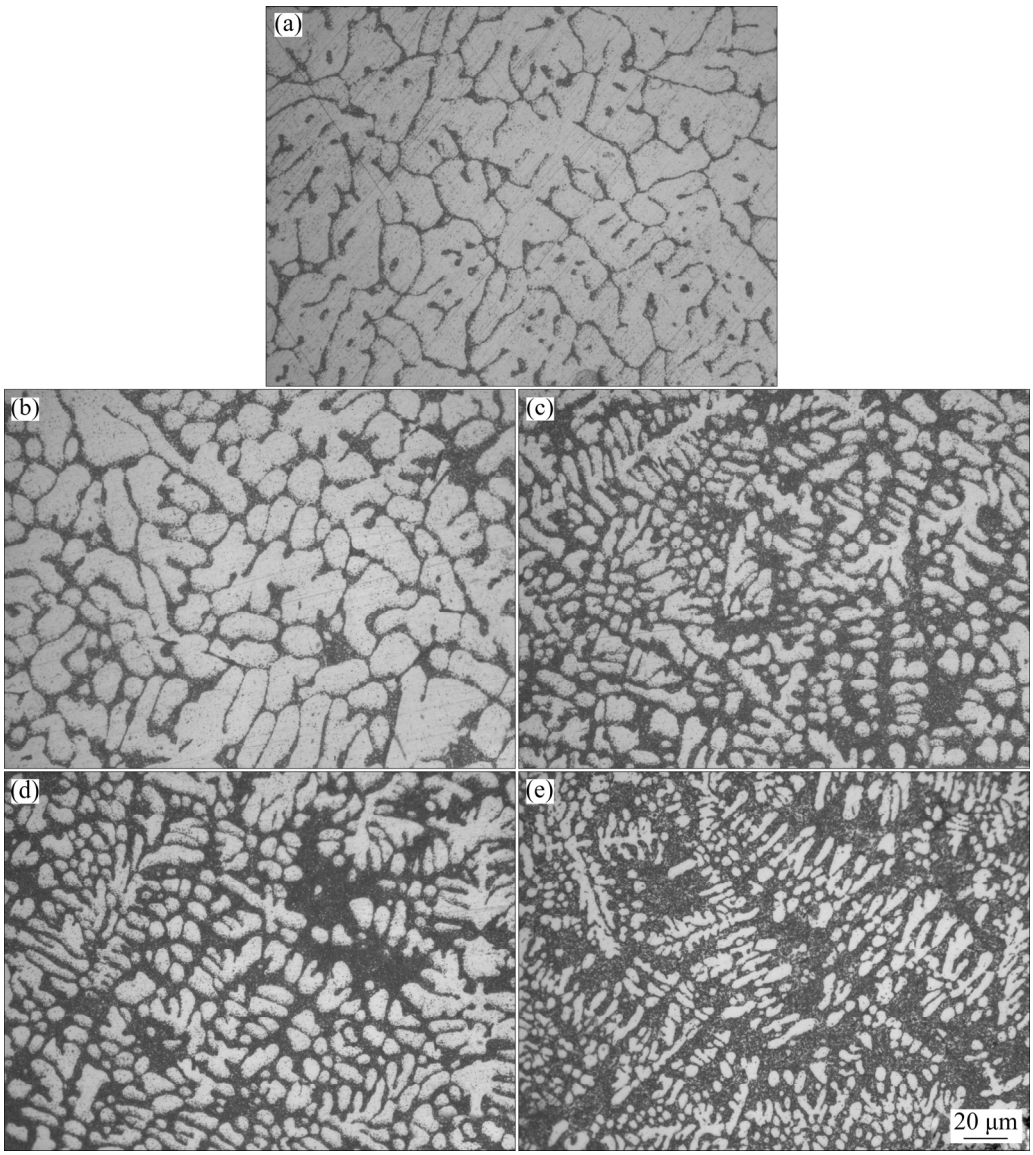

Fig. 2 OM images of α(Al) dendritic morphologies in Sr-modified Al−Si alloys: (a) Al−3Si; (b) Al−5Si; (c) Al−7Si; (d) Al−9Si; (e) Al−12Si

seen that with the Si content increasing, the proportion of eutectic structure increased, as well as the dendrite gap. The dendrite gap in each alloy was measured and summarized in Fig. 3. At the Si contents of 3 wt.% and 5 wt.%, the average dendrite gaps were 2.3 and 3.7 μm, respectively. At the Si content more than 5 wt.%, the dendrite gap increased significantly, and the primary dendrite gap was much larger than secondary dendrite gap. To achieve a clearer comparison, only the secondary dendrite gaps were counted in Figs. 2(c−e). The statistics suggested that when the Si contents were 7 wt.%, 9 wt.% and 12 wt.%, the average secondary dendrite gaps reached 7.9, 8.9 and 8.8 μm, respectively, as shown in Fig. 3. This

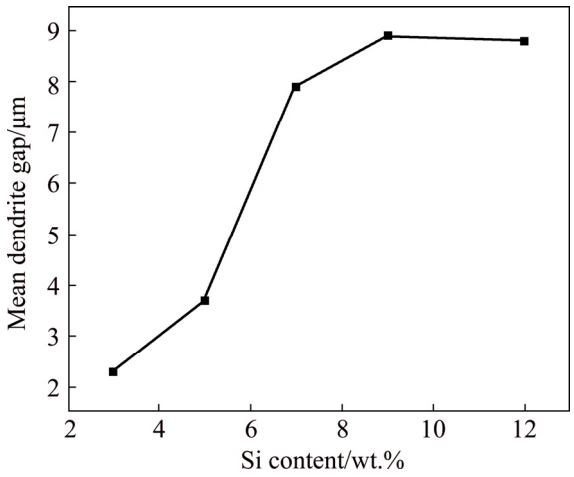

Fig. 3 Statistical results of dendrite gap in Sr-modified Al−Si alloys

indicated that when the Si content was 9 wt.%, the secondary dendrite gap reached a stable value.

The eutectic Si phase morphology was characterized by SEM. The observation results showed that the morphology and size of eutectic Si phases were nearly the same in all unmodified Al−Si alloys. Therefore, only the SEM image of Al−7Si alloy was presented in Fig. 4. Figure 4(a) showed that the eutectic Si phases were coarse flaky structure in unmodified Al−7Si alloy, and the maximum size of the coarse flaky eutectic Si phases was 20−30 μm. Figures 4(b)−(f) showed the morphologies of eutectic Si phases in Al−*x*Si (*x*=3, 5, 7, 9 and 12) alloys modified by 0.05 wt.% Sr. Compared with Fig. 4(a), the morphologies of eutectic Si phases changed significantly in Figs. 4(b)−(f). Most of the eutectic Si phases were transformed into fibrous structure with a diameter of 0.2−0.3 μm, and the end of fibrous eutectic Si phases was approximately hemispherical. Most of adjacent fibrous eutectic Si phases were parallel to each other. In addition, a small amount of eutectic Si phases were fine flaky structure, and the maximum length of the fine flaky eutectic Si phases was between 2 and 5 μm. The proportion of fine flaky eutectic Si phases was different with the Si content increasing.

Figure 4(b) illustrated that a certain amount of fine flaky eutectic Si phases (indicated by arrows) were adjacent and approximately parallel to each other in Sr-modified Al−3Si alloy. Likewise, there were also a certain amount of fine flaky eutectic Si phases in Sr-modified Al−5Si alloy. The eutectic Si phases indicated by arrows were fine flaky structure and almost parallel to each other, as presented in Fig. 4(c). On both sides of fine flaky Si phases,

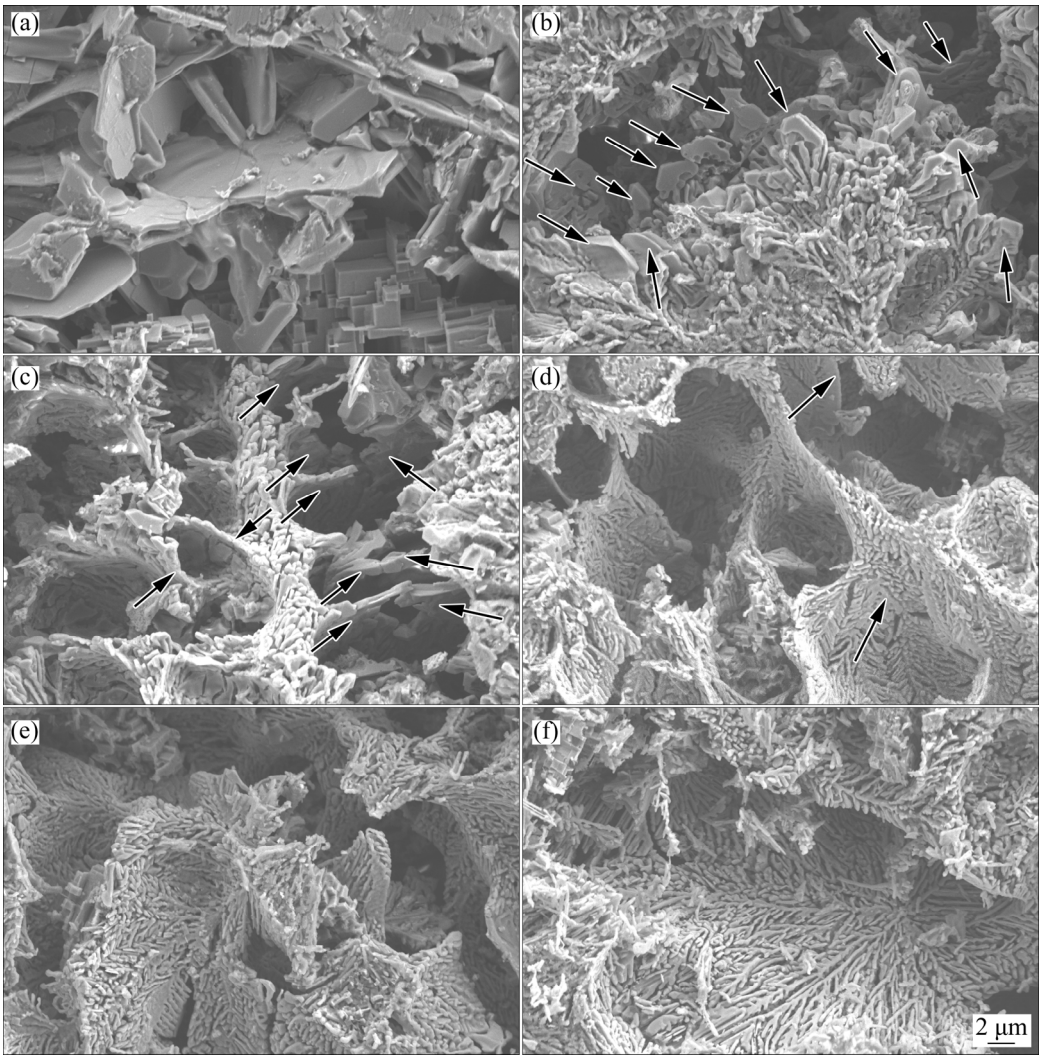

Fig. 4 SEM images of eutectic Si phases in unmodified Al−7Si alloy (a) and Sr-modified Al−*x*Si alloys (*x*=3, 5, 7, 9 and 12): (b) Al−3Si; (c) Al−5Si; (d) Al−7Si; (e) Al−9Si; (f) Al−12Si

approximately dendrite-like holes were left when the dendrites were fully etched. This indicated that most flaky eutectic Si phases were precipitated between the dendrites with a small gap.

When the Si content increased to 7 wt.% (Fig. 4(d)), the eutectic Si phases were mainly fibrous structure, and the proportion of fine flaky eutectic Si phases was obviously smaller than that of Sr-modified Al−3Si and Al−5Si alloys. Moreover, Fig. 4(d) showed that the flaky eutectic Si phases (indicated by arrows) were far away from each other, and were not parallel to each other. There were considerable fibrous eutectic Si phases between flaky eutectic Si phases.

Figures 4(e) and (f) showed that it was difficult to observe fine flaky eutectic Si phases, and the eutectic Si phases were almost fibrous when Si contents were 9 wt.% and 12 wt.%, respectively.

In this study, the proportion of fine flaky eutectic Si phases was used for judging the effect of Sr modification process. There were still a certain amount of fine flaky Si phases in Sr-modified alloys when Si content was low, and thereby the effect of Sr modification process was weak. With the Si content increasing, the proportion of fine flaky Si phases gradually decreased, and thereby the effect of Sr modification process gradually increased. When the Si contents were 9 wt.% and 12 wt.%, respectively, it was difficult to observe fine flaky eutectic Si phases, and thereby Sr indicated an excellent modification effect.

4 Discussion

The electrical resistivity of Si phase is 11 orders of magnitude higher than that of pure Al at room temperature, and thereby the free electrons were very hard to pass through the eutectic Si phases. Therefore, the decrease of thermal conductivity should be related to the precipitation of high resistance eutectic Si phases that would hinder electrons transport in alloys. In addition, it suggested from experiment results that the increment and increasing rate of thermal conductivity of Sr-modified alloys were improved with the Si content increasing. The proportion of fine flaky Si phases in alloys with low Si content (≤5 wt.%) was higher than that of high Si content (≥7 wt.%). Thus, the improvement of thermal conductivity of Sr-modified alloys should be closely associated with the morphological variation of eutectic Si phases.

4.1 Effect of solidification on morphology of Si phases

For the hypoeutectic Al−Si binary alloy, the solidification is divided into two stages: $L\rightarrow$ α(Al) and $L\rightarrow\alpha$(Al)+Si, respectively. The α(Al) dendrites are precipitated in the former stage. The eutectic structure is precipitated in the later stage, and the morphology of eutectic Si phases is coarse flake. Sr modification process could change the morphology of eutectic Si phases [10−12]. Moreover, some studies [21,22] found that the fibrous eutectic Si branches originate from the trunk at the same angle (70.5°) in Sr-modified Al−Si alloys, so the mentioned adjacent fibrous eutectic Si branches are parallel to each other. However, in this study it was found that although most of eutectic Si phases were transformed into fibrous structure by Sr modification process, there were a certain amount of fine flaky Si phases between α(Al) dendrites. The proportion of fine flaky eutectic Si phases decreased with the Si content increasing.

The primary α(Al) solidification reaction was prior to α(Al)+Si eutectic reaction. During the eutectic reaction, the melt would solidify between α(Al) dendrites. Therefore, the dendrite gap and the solute distribution between the dendrites would affect α(Al)+Si eutectic reaction, especially the morphology of eutectic Si phases.

During the growth of primary α(Al), solute elements were continuously discharged at front of solid/liquid (S/L) interface. This would lead to solute enrichment at the front of S/L interface and form a diffusion field, resulting in constitutional undercooling (ΔT_c) [23−25]. From the onset of eutectic reaction, the diffusion field near the S/L interface of α(Al) dendrites would have a continuous effect on eutectic reaction [26−28]. When the solute diffusion fields between two adjacent α(Al) dendrites overlapped each other, the solute concentration gradient would decrease, and ΔT_c would in turn decrease. In the eutectic reaction, some eutectic Si phases nucleated on or near the primary α(Al) surface [26−28]. When ΔT_c was reduced to a critical undercooling (ΔT_{cri}), the eutectic Si phases that nucleated on or near the

primary α(Al) surface and grew in the overlapping area of the diffusion field would grow in the form of fine flake [29].

Figure 3 showed that the average dendrite gap gradually increased with the Si content increasing. Therefore, in Sr-modified alloys, the overlapping area of the inter-dendrite diffusion field would decrease with the Si content increasing, and the area of the critical undercooling (ΔT_{cri}) required for the precipitation of flaky eutectic Si phases would in turn decrease. As a result, the precipitation probability for fine flaky eutectic Si phases became smaller, especially for those adjacent and parallel to each other.

4.2 Effect of Si phase morphology on thermal conductivity

According to Matthiessen's rule, the resistivity can be expressed as [30,31]

$$\rho=\rho_T+\rho_R \quad (1)$$

$$\rho_R=\rho_{gb}+\rho_d+\rho_{ss}+\rho_p \quad (2)$$

where ρ is the electrical resistivity of metallic materials; ρ_T is the basic resistivity, and only related to temperature; ρ_R is the residual resistivity, which was related to the microstructure and was the sum of four resistivity; ρ_{gb} denotes the resistivity induced by the grain boundary; ρ_d represents electron scattering by dislocations; ρ_{ss} and ρ_p are the resistivity components due to the solute atoms and precipitates phase, respectively. Only when the grain size close to the average free path of free electrons will the effect of ρ_{gb} on the resistivity be obvious [32]. The average free path of free electrons is in the order of nanometer [33], and the size of Al grains is in the order of micrometer or millimeter. Therefore, the effect of ρ_{gb} on the resistivity is negligible. The effect of ρ_d on the resistivity is slight at room temperature [30,34]. The cooling conditions were the same for all alloys, and thereby the solid solubility of Si in Al matrix was almost the same for unmodified and Sr-modified Al−Si alloys. Therefore, the improvement of thermal conductivity of Sr-modified alloys was mainly related to ρ_p.

Some researchers [30,35,36] found that the interface between matrix and secondary phase can scatter free electrons and shorten the average free path of electrons. The cross-section dimensions of secondary phase significantly affect the resistivity (ρ) of alloys, and the resistivity increases with *P/S* increasing, where *P* and *S* refer to the perimeter and the cross-section area of the second phase, respectively. From the mentioned finding, the influence law of secondary phase morphology on the electrical conductivity and thermal conductivity can be inferred.

TIMPLE et al [37−39] characterized the overall 3D morphologies of the eutectic Si phases in unmodified and Sr-modified Al−Si alloys by means of FIB-EsB tomography. They found that the overall 3D morphology of unmodified eutectic Si phases was flaky structure, and the overall 3D morphology of Sr-modified eutectic Si phases was a mixed morphology of fibrous structure and flaky structure. This is consistent with the results of this study, as shown in Fig. 3. Therefore, the cross-section of flaky Si phases is rectangular with a large aspect ratio, and the radial cross-section of fibrous Si phases is approximately circular.

From the mentioned analysis, it can be speculated that at the identical Si content, the thermal conductivity of Sr-modified Al−Si alloys is higher than that of unmodified Al−Si alloys since the *P/S* ratio of the circular cross-section is higher than that of rectangle cross-section. It can be further speculated that the increment and increasing rate of thermal conductivity should be improved with the decreasing proportion of flaky eutectic Si phases. These speculations were confirmed by experiment results of this study. But, the mechanism of interface to scatter free electrons is worthy of a deep analysis.

Though both eutectic Si phase and α(Al) phase dissolved a small amount of solute, their thermo-physical properties were close to those of pure Si and Al, respectively. The linear expansion coefficients of pure Al and Si were significantly different, as listed in Table 2 [4,40]. As revealed from the data in Table 2, in the temperature range of 400−800 K, the ratio of linear expansion coefficients of Al and Si was 7.3−8.1. Thus, as impacted by the difference in shrinkage between the α(Al) phase and the eutectic Si phase in the cooling process, thermal strains would be generated at Al/Si interface. It is noteworthy that the thermal strains on the α(Al) phase side would lead to the formation of lattice distortion layers. The lattice distortion layer would have a significant effect on the length of electron mean free paths.

Table 2 Linear expansion coefficients of pure Al and Si at different temperatures [4,40]

T/K	α(Al)/10^{-6} K^{-1}	α(Si)/10^{-6} K^{-1}	α(Al)/α(Si)
400	24.9	3.253	7.7
500	26.5	3.614	7.3
600	28.2	3.842	7.3
700	30.4	4.016	7.6
800	33.5	4.151	8.1

The lattice structure of Al phase (FCC crystal structure) is different from that of Si (diamond crystal structure), and the lattice constant of Al (0.45 Å) is also quite different from the of Si (0.54 Å), and the former is 20% smaller than the latter. So, it is difficult to form a coherent interface. Therefore, a large number of crystal defects (e.g. vacancy and dislocation) would be generated in the lattice distortion layer of α(Al) phase.

In accordance with Bloch theorem [41], free electron mobility is maximized in a perfect atomic lattice. Any strains, imperfections, or bulk defects in the material act as free electron scattering centers, which reduce their mean free paths and hence the conductivity [18]. Accordingly, the lattice distortion layer will scatter free electrons. The scattering effect is related to the transport path length of free electrons in lattice distortion layers, and the scattering effect increases with the increment of electrons transport path length.

At room temperature, the resistivity of Si is 11 orders of magnitude greater than that of Al, and thereby Si phases could be regarded as an insulator. Therefore, free electrons would be reflected by eutectic Si phases after passing through the lattice distortion layer. The transport path length (L) (L=L_i +L_r, where L_i is the length of incident path, and L_r is the length of reflection path) of free electrons in lattice distortion layer is related to many factors, among which the interface shape is the most important factor. Figure 5 presented the schematic diagram that free electrons transport at plane and circular interfaces, and the blue area indicated the lattice distortion layer in α(Al) phase.

Since the cooling conditions of all alloys were identical, the thickness of the lattice distortion layer of unmodified and Sr-modified alloys could be regarded as the same. When the free electron incident angle (i) and the lattice distortion layer thickness (δ) were the same, the length of incident path L_i of free electron at planar interface would be longer than that at circular interface. The difference in the two incident paths was ΔL_i (shown in Fig. 5(b)). Similarly, the length of reflection path L_r of free electron at plane interface would also be longer than that at the circular interface, and the difference in two reflection path was ΔL_r. Therefore, the difference in transport path length at the two different interfaces was expressed as ΔL (ΔL=ΔL_i+ΔL_r). It could be inferred that the fibrous eutectic Si phases could effectively reduce transport path length of free electrons in lattice distortion layers.

In this study, at the interface of unit area, the average difference in transport path length at the two different interfaces for all of the electrons was defined as average ΔL. Since the incident angle i of free electrons was random in all alloys, the average ΔL was only related to the radius (R) of fibrous eutectic Si phases. As discussed in Section 3.2, the diameter of fibrous eutectic Si phases in all Sr-modified Al−Si alloys was similar, so the fibrous eutectic Si phases exerted the same effect on decreasing the average ΔL in all Sr-modified alloys.

In addition, fibrous eutectic Si phases could also decrease the probability of free electron scattering. Under the same electron incidence angle i and incidence cross-section area (D×W, D and W are the length and width of the cross-section, respectively), the probability of free electrons scattering on flaky eutectic Si phases is greater than that of fibrous eutectic Si phases, since there are lots of gaps between fibrous Si branches, as shown in Figs. 6(a) and (b). Additionally, the probability of free electrons scattering between adjacent two parallel flaky eutectic Si phases was greater than that between two adjacent parallel fibrous eutectic Si branches, as shown in Figs. 6(c) and (d). From the above analysis, it could be seen that flaky eutectic Si phases could decrease the probability of free electron scattering. WENG et al [42] also believed that the fibrous Si phases could effectively reduce the probability of electron scattering after studying the thermal conductivity of Sr-modified Al−Si alloys.

In brief, fibrous eutectic Si phases could shorten the transport path length of free electrons in lattice distortion layer, and reduce the probability of

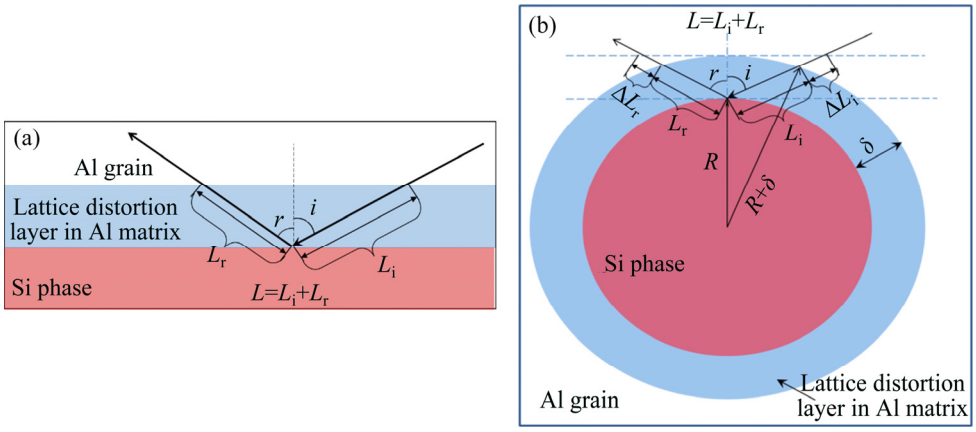

Fig. 5 Path of electron scattering at α(Al)/Si interface with different shapes: (a) Planar interface; (b) Circular interface

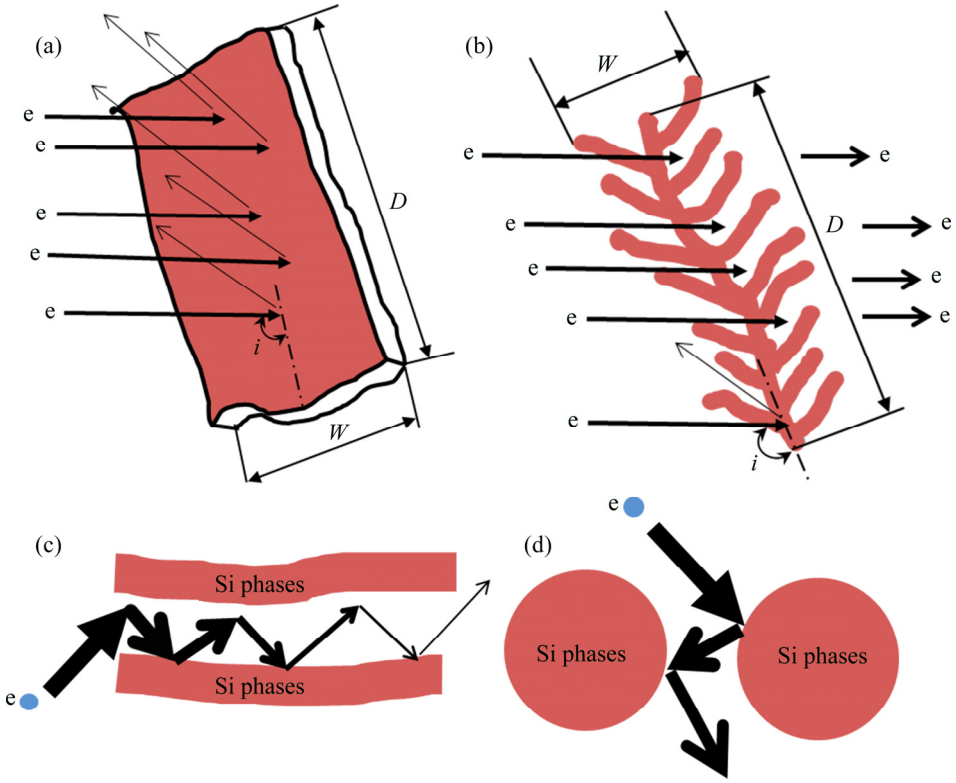

Fig. 6 Scattering of free electrons on different eutectic Si phases: (a) Single flaky eutectic Si phase; (b) Single fibrous eutectic Si phase; (c) Adjacent two parallel flaky eutectic Si phases; (d) Adjacent two parallel fibrous eutectic Si branches

free electrons scattering at the interface. Thus, the improvement of thermal conductivity for Sr-modified alloys was primarily related to the morphology variation of eutectic Si phases.

Under the same Si content, the density of eutectic Si phase in unmodified and Sr-modified alloys was almost the same. With the Si content increasing in Sr-modified alloys, the proportion of flaky eutectic Si phases decreased, especially the proportion of flaky Si phases parallel to each other decreased significantly. On the contrast, the proportion of fibrous Si phases gradually increased. Therefore, compared with unmodified Al−Si alloys, the increment and increasing rate of the thermal conductivity of Sr-modified alloys were improved with the Si content increasing. When the Si content was 9 wt.%, it was difficult to observe the flaky eutectic Si phases, and thereby the increment and

increasing rate were 33.5 W/(m·K) and 25.2%, respectively, and tended to be stable as Si content further increased.

5 Conclusions

(1) The thermal conductivity of hypoeutectic Al−Si alloys was improved by Sr modification process. The increment and increasing rate of thermal conductivity were gradually increased with the Si content increasing，and tended to be stable as Si content was 9 wt.%.

(2) In Sr-modified hypoeutectic Al−Si alloys, the eutectic Si phase was a mixture of fibrous structure and fine flaky structure, and the proportion of the fine flaky eutectic Si phases gradually decreased with the Si content increasing. When the Si content reached 9 wt.%, the proportion of fine flaky eutectic Si phases was nearly negligible.

(3) The precipitation of fine flaky eutectic Si phases was related to the narrow dendrites gap in Sr-modified alloys. With the Si content increasing, the average secondary dendrite gap gradually increased. When the Si content was 9 wt.%, the average secondary dendrite gap tended to be stable.

(4) The transformation of eutectic Si phase morphology from flake to fiber was beneficial to improving the thermal conductivity. The fibrous eutectic Si phases could shorten the transport path length of free electrons in lattice distortion layer, and reduce the probability of free electron scattering on interface.

References

[1] BRANDT R, NEUER G. Electrical resistivity and thermal conductivity of pure aluminum and aluminum alloys up to and above the melting temperature [J]. International Journal of Thermophysics, 2007, 28(5): 1429−1446.

[2] CUI Xiao-li, WU Yu-ying, LIU Xiang-fa, ZHAO Qing-ru, ZHANG Guo-jun. Effects of grain refinement and boron treatment on electrical conductivity and mechanical properties of AA1070 aluminum [J]. Materials & Design, 2015, 86: 397−403.

[3] HATCH J E. Aluminum: Properties and physical metallurgy [M]. Ohio: American Society for Metals, 1984.

[4] WANG Zhu-tang, TIAN Rong-zhang. Aluminum alloy and processing manual [M]. 3rd ed. Changsha: Central South University Press, 216−234. (in Chinese)

[5] STADLER F, ANTREKOWITSCH H, FRAGNER W, KAUFMANN H, PINATEL E R, UGGOWITZER P J. The effect of main alloying elements on the physical properties of Al−Si foundry alloys [J]. Materials Science and Engineering A, 2013, 560: 481−491.

[6] CHEN J K, HUNG H Y, WANG C F, TANG N K. Effects of casting and heat treatment processes on the thermal conductivity of an Al−Si−Cu−Fe−Zn alloy [J]. International Journal of Heat and Mass Transfer, 2017, 105: 189−195.

[7] LIN Gao-yong, LI Kun, FENG Di, FENG Yong-ping, SONG Wei-yuan, XIAO Meng-qiong. Effects of La−Ce addition on microstructure and mechanical properties of Al−18Si−4Cu−0.5 Mg alloy [J]. Transactions of Nonferrous Metals Society of China, 2019, 29: 1592−1600.

[8] PENG Hao-ping, LI Zhi-wei, ZHU Jia-qing, SU Xu-ping, LIU Ya, WU Chang-jun, WANG Jian-hua. Microstructure and mechanical properties of Al−Si alloy modified with Al−3P [J]. Transactions of Nonferrous Metals Society of China, 2020, 30: 595−602.

[9] QIU Ke, WANG Ri-chu, PENG Chao-qun, WANG Nai-guang, CAI Zhi-yong, ZHANG Chun. Effects of Mn and Sn on microstructure of Al−7Si−Mg alloy modified by Sr and Al−5Ti−B [J]. Transactions of Nonferrous Metals Society of China, 2015, 25: 3546−3552.

[10] LIN Y C, LUO Shun-cun, JIANG Xing-you, TANG Yi, CHEN Ming-song. Hot deformation behavior of a Sr-modified Al−Si−Mg alloy: Constitutive model and processing maps [J]. Transactions of Nonferrous Metals Society of China, 2018, 28: 592−603.

[11] FARAHANY S, OURDJINI A, BAKHSHESHI-RAD H R. Microstructure, mechanical properties and corrosion behavior of Al−Si−Cu−Zn−X (X= Bi, Sb, Sr) die cast alloy [J]. Transactions of Nonferrous Metals Society of China, 2016, 26: 28−38.

[12] ACHARYA M, MANDAL A. Individual and synergistic effect of gamma alumina (γ-Al_2O_3) and strontium on microstructure and mechanical properties of Al−20Si alloy [J]. Transactions of Nonferrous Metals Society of China, 2019, 29: 1353−1364.

[13] WEN Cheng, GAN Jun-qi, LI Cheng-bo, HUANG Yu-jian, DU Jun. Comparative study on relationship between modification of Si phase and thermal conductivity of Al–7Si alloy modified by Sr/RE/B/Sb elements [J]. International Journal of Metalcasting, Published online: 13 March 2020. https://doi.org/10.1007/s40962-020-00436-z

[14] GAN Jun-qi, HUANG Yu-jian, DU Jun, WEN Cheng, LIU Jing. Synchronous improvement in thermal conductivity and mechanical properties of Al−7Si−0.6Fe−0.5Zn cast alloy by B/La/Sr composite modification [J]. Materials Research Express, 2020, 7: 086501.

[15] MAXWELL J C. A treatise on electricity and magnetism [M]. Cambridge: Oxford University Press, 1904.

[16] CHEN J K, HUNG H Y, WANG C F, TANG N K. Thermal and electrical conductivity in Al−Si/Cu/Fe/Mg binary and ternary Al alloys [J]. Journal of Materials Science, 2015, 50: 5630−5639.

[17] MULAZIMOGLU M H, DREW R A L, GRUZLESKI J E. The effect of strontium on the electrical resistivity and conductivity of aluminum−silicon alloys [J]. Metallurgical Transactions A, 1987, 18: 941−947.

[18] VANDERSLUIS E, EMADI P, ANDILAB B, RAVINDRAN C. The role of silicon morphology in the electrical conductivity and mechanical properties of as-cast B319 aluminum alloy [J]. Metallurgical and Materials Transactions A, 2020, 51: 1874−1886.

[19] AKOSHIMA M, HAY B, NEDA M, GRELARD M. Experimental verification to obtain intrinsic thermal diffusivity by laser-flash method [J]. International Journal of Thermophysics, 2013, 34(5): 778−791.

[20] ZHOU C, JI G, CHEN Z, WANG M L, ADDAD A, SCHRYVERS D, WANG H W. Fabrication, interface characterization and modeling of oriented graphite flakes/Si/Al composites for thermal management applications [J]. Materials and Design, 2014, 63: 719−728.

[21] TIMPEL M, WANDERKA N, SCHLESIGER R, YAMAMOTO T, LAZAREV N, ISHEIM D, SCHMITZ G, MATSUMMRA S, BANHART J. The role of strontium in modifying aluminium−silicon alloys [J]. Acta Materialia, 2012, 60(9): 3920−3928.

[22] TIMPLE M, WANDERKA N, SCHLESIGER R, YAMAMOTO T, ISHEIM D, SCHMITZ G, MATSUMURA S, BANHART J. Sr−Al−Si co-segregated regions in eutectic Si phase of Sr-modified Al−10Si alloy [J]. Ultramicroscopy, 2013, 132: 216−221.

[23] EASTON M, STJOHN D. An analysis of the relationship between grain size, solute content, and the potency and number density of nucleant particles [J]. Metallurgical and Materials Transactions A, 2005, 36: 1911−1920.

[24] STJOHN D H, QIAN M, EASTON M A, CAO P. The interdependence theory: The relationship between grain formation and nucleant selection [J]. Acta Materialia, 2011, 59(12): 4907−4921.

[25] STJOHN D H, EASTON M A, QIAN M, CAO P, BIRMINGHAM M J. Introduction to the interdependence theory of grain formation and its application to aluminium, magnesium and titanium alloys [J]. Materials Science Forum, 2011, 690: 206−209.

[26] DAHLE A K, NOGITA K, ZINDEL J W, MCDONALD S D, HOGAN L M. Eutectic nucleation and growth in hypoeutectic Al−Si alloys at different strontium levels [J]. Metallurgical Materials Transactions A, 2001, 32(4): 949−960.

[27] HEIBERG G, ARNBERG L. Investigation of the microstructure of the Al−Si eutectic in binary aluminium−7wt%silicon alloys by electron backscatter diffraction (EBSD) [J]. Journal of Light Metals, 2001(1): 43−49.

[28] NOGITA K, MCDONALD S D, DAHLE A K. Solidification mechanisms of unmodified and strontium-modified hypereutectic aluminium−silicon alloys [J]. Philosophical Magazine, 2004, 84(17): 1683−1696.

[29] DARLAPUDI A, MCDONALD S D, TERZI S, PRASAD A, FELBERBAUM M, STJOHN D H. The influence of ternary alloying elements on the Al−Si eutectic microstructure and the Si morphology [J]. Journal of Crystal Growth, 2016, 433: 63−73.

[30] TIAN L, ANDERSON I, RIEDEMANN T, RUSSELL A. Modeling the electrical resistivity of deformation processed metal−metal composites [J]. Acta Materialia, 2014, 77: 151−161.

[31] MACDONALD D K C, SARGINSON K. Size effect variation of the electrical conductivity of metals [J]. Proceedings of the Royal Society A, 1950, 203: 223−240.

[32] MAYADAS A F, SHATZKES M. Electrical-resistivity model for polycrystalline films: The case of arbitrary reflection at external surfaces [J]. Physical Review B, 1970, 1(4): 1382−1389.

[33] HANAOKA Y, HINODE K, TAKEDA K, KODAMA D. Increase in electrical resistivity of copper and aluminum fine lines [J]. Materials Transactions, 2002, 43(7): 1621−1623.

[34] KOCER M, SACHSLEHNER F, MULLER M, SCHAFLER E, ZEHETBAUER M. Measurement of dislocation density by residual electrical resistivity [J]. Materials Science Forum, 1996, 210−213: 133−140.

[35] DINGLE R B. The electrical conductivity of thin wires [J]. Proceedings of the Royal Society A, 1950, 201: 540−545.

[36] HERINGHAUS F, SCHNEIDER-MUNTAU H, GOTTSTEIN G. Analytical modeling of the electrical conductivity of metal matrix composites: Application to Ag−Cu and Cu−Nb [J]. Materials Science and Engineering A, 2003, 347: 9−20.

[37] TIMPLE M, WANDERKA N, MURTY B S, BANHART J. Three-dimensional visualization of the microstructure development of Sr-modified Al−15Si casting alloy using FIB-EsB tomography [J]. Acta Materialia, 2010, 58: 6600−6608.

[38] TIMPLE M, WANDERKA N, VINOD KUMAR G S BANHART J. Microstructural investigation of Sr-modified Al−15wt.%Si alloys in the range from micrometer to atomic scale [J]. Ultramicroscopy, 2011, 111: 695−700.

[39] TIMPLE M, WANDERKA N, SCHLESIGER R, YAMAMOTO T, ISHEIM D, SCHMITZ G, MATSUMURA S, BANHART J. Sr−Al−Si co-segregated regions in eutectic Si phase of Sr-modified Al−10Si alloy [J]. Ultramicroscopy, 2013, 132: 216−221.

[40] SWENSON C A. Recommended values for the thermal expansivity of silicon from 0 to 1000 K [J]. Journal of Physical and Chemical Reference Data, 1983, 12(2): 179−182.

[41] KITTEL C. Introduction to solid state physics [M]. XIANG Jin-zhong, WU Xing-hui, Trans. Beijing: Chemical Industry Press, 2005: 119. (in Chinese)

[42] WENG W P, NAGAUMI H, SHENG X D, FAN W Z, CHEN X C, WANG X N. Influence of silicon phase particles on the thermal conductivity of Al−Si alloys [J]. Light Metals, 2019: 193−198.

Sr 变质对亚共晶 Al−Si 合金显微组织和导热系数的影响

甘俊旗，黄玉剑，温 澄，杜 军

华南理工大学 材料科学与工程学院，广州 510640

摘 要：在亚共晶 Al−Si(3%−12%Si，质量分数)合金中加入微量 Sr(0.05%，质量分数)改善合金的显微组织并提高其导热系数。研究结果表明，采用 Sr 变质工艺能提高亚共晶 Al−Si 合金的导热系数，且随着 Si 含量的增加，导热系数的增加幅度和增加率逐渐增大。导热系数的提高主要与共晶 Si 相的形貌变化有关。在 Sr 变质 Al−Si 合金中，共晶 Si 相的形貌为纤维状和细片状混合形貌。随着 Si 含量的增加，细片状共晶 Si 相的比例逐渐减小。当 Si 含量达到 9%(质量分数)时，Sr 变质合金中细片状共晶 Si 相的比例可以忽略不计。相应地，Sr 变质合金导热系数的增加幅度和增加率达到最大，并趋于稳定。

关键词：亚共晶 Al−Si 合金；Sr 变质；共晶 Si 相形貌；导热系数；Al/Si 界面

(Edited by Wei-ping CHEN)